❏   331

Design and development of a modular magnetic wheeled robot for out-pipe inspection

Sugin Elankavi Rajendran[1,2], Kuppan Chetty Ramanathan[3], Harish Kumar Guasekaran[3], Arun Kumar Pinagapani[4], Dinakaran Devaraj[5], Ramya Mathanagopal[6]

[1]Centre for Industrial Automation, Chennai Institute of Technology, Chennai, Tamil Nadu, India
[2]Centre for Automation and Robotics, Hindustan Institute of Technology and Science, Chennai, Tamil Nadu, India
[3]School of Mechanical Engineering, SASTRA Deemed to be University, Thanjavur, India
[4]School of Electrical and Electronics Engineering, SASTRA Deemed to be University, Thanjavur, India
[5]Haystack Robotics, Chennai, India
[6]School of Computing Sciences, Agurchand Manmull Jain College, Tamil Nadu, India

Article Info

ABSTRACT

This paper presents the design of a modular mobile robot capable of climbing and inspecting vertical ferromagnetic pipes using magnetic wheels. Mobile robots used for climbing ferromagnetic surfaces employ magnetic tracks, wheels, and magnets attached to the robot's body. When it comes to ferromagnetic pipes, magnetic wheels and magnets attached to the body can be used. Among them, magnetic wheels are commonly used for inspecting ferromagnetic pipes. While current robots are suitable for large pipes, they are not practical for smaller ones. To address this gap, a small-sized robot equipped with a magnetic wheel system that ensures both strong attachment and smooth movement along vertical ferromagnetic surfaces is developed. The robot's magnetic adhesion performance was analyzed through simulations using finite element method magnetics and validated through laboratory experiments. The results show an average error of only 8.25% between simulation and real-world tests, confirming the system's reliability for external pipe inspection.

Corresponding Author:

Kuppan Chetty Ramanathan
School of Mechanical Engineering, SASTRA Deemed to be University
Thanjavur, Tamil Nadu, 613401, India
Email: kuppanchetty@mech.sastra.edu

1. INTRODUCTION

Pipeline inspection robots have received abundant attention in the industrial sector as a result of recent technological advances. This is due to their wide use in maintenance and inspection applications like detecting cracks, corrosion, and ageing. Since it is dangerous for humans to climb high-altitude pipes, pipeline inspection robots are used to do their jobs. Pipeline inspections are done in two ways: one is in-pipe inspection [1], [2], and the other is out-pipe inspection [3], [4]. The in-pipe robots have seen developments in the past decade, and their mobility inside the pipeline was studied in [5]–[7]. The flow inside the pipelines should be stopped to deploy in-pipe inspection robots. Therefore, industries prefer out-pipe inspection robots because it does not need to stop the flow in pipelines [8]. Industries have pipelines in high-altitude places and require robots that can climb vertical pipes. Vertical motion has different types of adhesion systems, which are divided into five different types [9], [10]. Adhesion methods consist of biometric [11], [12], vacuum suction [13], rail-guided [14], [15], gripping [16], and magnetic [17].

The biometric adhesion in [18] consists of geckos that provide the necessary stickiness. It uses micro hair patches to stick to surfaces. Vacuum suction uses pressure difference with the help of suction cups to provide the required adhesion force [13], [19]. It is the most commonly used type of adhesion among others and is not limited to a particular surface. It can be used on glass, tiles, steel, and concrete surfaces. The rail-guided adhesion [15] uses rails to gain the necessary traction for moving the robot vertically. The rails help the robot hold onto the surface and slide along it, preventing the robot from falling. In uneven surfaces and sophisticated environments, the gripping type is most suitable for providing the necessary adhesion. Robots using the grip mechanism are commonly used in places where force monitoring is required [16]. The limitation of vacuum-type adhesion is that it can only provide the necessary adhesion on smooth surfaces. The limitation of the gripping type and rail type is that it is restricted to a particular region but have a high payload carrying capacity, and the biometric type has a very low payload carrying capacity [9].

Ferromagnetic pipes are widely used in the petroleum, energy, and chemical industries [20]. Vertical motion in ferrous surfaces plays an important role in designing and developing a pipeline inspection robot [9]. Magnetic adhesion, typically using permanent magnets as wheels, tracks, or body attachments, enables vertical mobility. This method offers advantages such as high payload capacity, power-free operation, and safety during power loss. Among various adhesion methods, magnetic wheels are preferred, as body-mounted magnets can induce significant structural stress [17], [21].

Out-pipe robots use a gripping mechanism, or the robots are made bigger than the outer diameter of the pipe, and thus the size of the robot increases as the pipeline circumference increases [3], [4], [22]. Enormous research is done on magnetic wheeled robots on concave surfaces [23], and they are used for in-pipe inspection. However, the research on magnetic wheeled robots on convex surfaces (out-pipe robots) is limited. Therefore, in this work, the focus is on developing a compact robot that can maneuver over out-pipes (convex surfaces).

This paper presents the design, simulation, and fabrication of cilampi, a modular magnetic wheeled robot for climbing vertical ferromagnetic pipes with diameters ≥200 mm. The robot's wheel mechanism ensures continuous contact with the pipe surface, adapting to varying curvatures. Cilampi can ascend vertically or follow a helical path for enhanced maneuverability. Magnetic adhesion force is analyzed using finite element method magnetics (FEMM) simulations and validated experimentally. The robot is powered by a 2200 mAh 1S LiPo battery, offering up to 44 minutes of operation in lab settings. This work addresses limitations in existing external pipeline inspection technologies.

2. MAGNETIC ADHESION USING FEMM

The magnetic adhesion force is determined using FEMM software. It is used for solving magnetic field problems [24]. The process involves modelling the geometry of the magnet with proper dimensions. The boundary conditions and the material properties are assigned to the respective systems. Then triangular mesh is used for computational accuracy, and using the FEMM solver, magnetic adhesion can be found. The visualization of flux density and the result interpretation can be done using the post-processing tools.

2.1 Selection of ring magnets

The ring magnet adhesion is based on the magnets' size, quality, and quantity. The ring type permanent magnet (PM) is made from neodymium-iron-boron (NdFeB) and is a powerful permanent magnet, the name of which begins with "N" followed by two numbers. The "N" represents Neodymium, and the two numbers indicate the maximum energy product in MegaGauss-Oersted (MGOe). The N52 grade magnet provides the best adhesion, but its market availability is limited. So, the N35 grade was chosen for this study due to its availability in the market. To determine the most suitable dimension of ring PM, simulations and analysis are performed on ring magnets with different inner diameters (ID), thicknesses, and stand-off distances.

2.2. Model creation and material selection

The FEMM software's built-in tools are utilised to draw a 2D diagram of the ring magnet and surface. The model is then surrounded by a circle, which acts as the boundary. The boundary serves as a geometric boundary for the analysis domain, separating the region of interest from the surrounding space. To avoid direct contact between the magnet and the surface, it is necessary to maintain a stand-off distance (SOD) of at least 0.5 mm [25]. If the magnet comes into contact with the surface, it will impede the wheel's movement, making it necessary to maintain a distance to allow for proper functioning.

The material for each component is selected after the model is created. The materials consist of a ferromagnetic pipe made of 1020 carbon steel, robot chassis and motor mount made of polylactic acid (PLA) [26], a magnetic wheel made of Aluminium 6061 and Neodymium N35 magnet. The material properties of

these materials are selected from the built-in library in FEMM software. The material selected for the robot chassis and the motor mount is polylactic acid (PLA). They are commonly used in 3D printing technology for fabricating components having less weight. This material is selected for the robot to decrease its weight, which reduces the payload of the robot. As mentioned earlier, the N35 is selected as the material for the ring magnet. The material for the ferromagnetic wall has been selected as 1020 steel, a commonly utilised material within various industries. Wang and Kawamura [27] have shown that a surface's thickness significantly impacts its magnetic adhesion properties, with thicker surfaces resulting in stronger adhesion.

In this simulation, the surface thickness is set to a minimum of 2 mm to evaluate the maximum magnetic adhesion force achievable. The ring magnet is modeled using 1020 steel properties [24], and air is assigned to the gap regions. Figure 1 illustrates the full model with material assignments. A fine triangular mesh with a size of 0.1 mm is used to capture geometric details accurately, ensuring precise field representation.
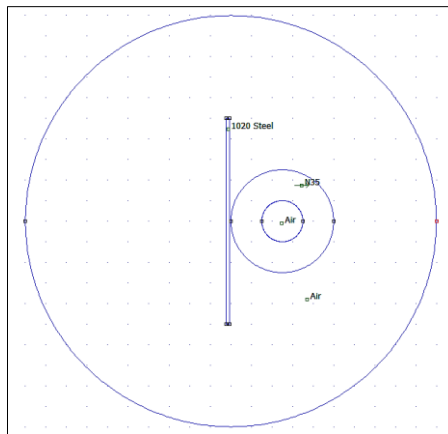

Figure 1. The entire model with the designated materials

2.3. Magnetic adhesion force for varying configurations of ring magnets as well as SOD

The magnetic adhesion force for different thicknesses of the ring magnet (RM), ID of the RM, wall thicknesses, and stand-off distances is computed using the method described above. Figure 2 shows magnetic adhesion for varying configurations of ring magnets. Simulation studies are conducted to assess the magnetic adhesion of ring magnets with internal diameters below 30 mm and thicknesses below 15 mm, which are the maximum sizes available in the market. The outer diameter of the ring magnet, set at a constant value of 50 mm, represents the maximum outer diameter available in the market. The ring magnets are positioned at a distance of 0.5 mm from the surface, with a constant surface thickness of 2 mm. These parameters are kept unchanged throughout the simulations.
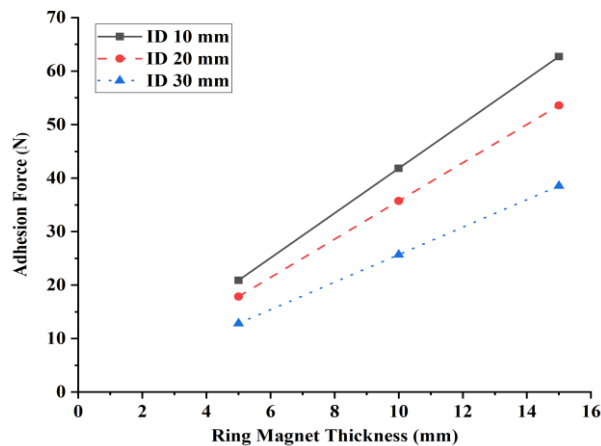

Figure 2. Magnetic adhesion force for varying configurations of RM

It is evident from Figure 2 that the magnetic adhesion force increases with magnet thickness and decreases with larger ID. The highest force (62.72 N) is achieved using a ring magnet with a 10 mm ID and 15 mm thickness, making it the optimal choice for further simulations. To optimize performance, simulations are conducted to study the effect of stand-off distance (SOD) on adhesion, varying SOD from 0.5 mm to 10 mm. The selected magnet has dimensions: 10 mm (ID), 50 mm (OD), and 15 mm (thickness), with a fixed wall thickness of 2 mm. Results are shown in Figure 3. The simulation results from Figure 3 demonstrate that as the Stand-off Distance increases, the magnetic adhesion force of the ring magnet decreases. The highest magnetic adhesion force of 62.72 N is obtained when the Stand-off Distance is at its minimum value of 0.5 mm.
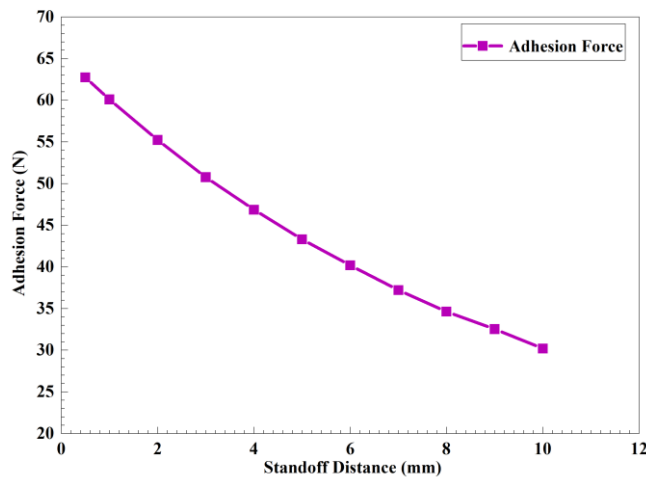

Figure 3. Magnetic adhesion force for varying SOD

2.4. Magnetic adhesion force of ring magnet for varying wall thickness

This simulation study aims to determine the wall thickness at which the adhesion force saturates. The adhesion force is calculated for the wall thickness from 1 mm to 15 mm, with the selected ring magnet of ID of 10 mm, outer diameter (OD) of 50 mm, thickness of 15 mm dimensions and with SOD of 0.5 mm. Figure 4 shows the magnetic adhesion force of the ring magnet for varying wall thicknesses.
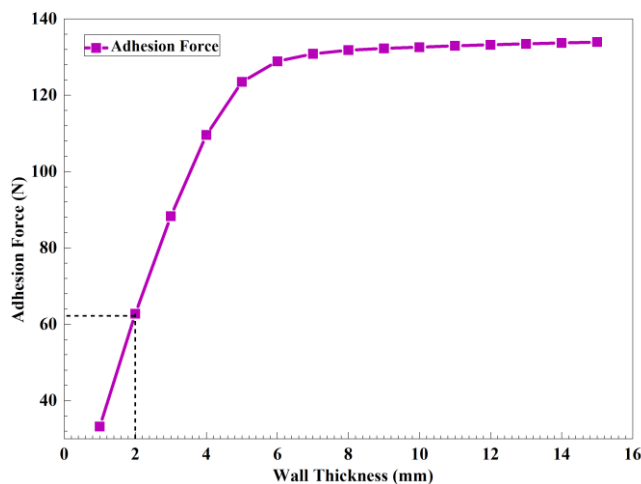

Figure 4. Magnetic adhesion force of ring magnet for varying wall thickness

It is evident from the result that beyond a wall thickness of 8 mm, the magnetic adhesion force nearly saturates at a value of 132 N. It also clearly shows that, based on the selected magnet, the adhesion

force is estimated to be 62.72 N when it is made to climb the wall with a thickness of 2 mm. It is well established that the magnetic adhesion force increases as the wall thickness increases until it reaches a point where the drastic increase in magnetic adhesion force ceases. Figure 4 also provides a relationship where the necessary wall thickness can be chosen based on the required adhesion for the magnet with an ID of 10 mm, OD of 50 mm, thickness of 15 mm and SOD of 0.5 mm.

3. FEMM SIMULATION AND DESIGN OF MAGNETIC WHEEL FOR CILAMPI

A magnetic wheel for the robot is designed to carry a payload of 1.5 kg while holding the permanent magnet. A robot with a payload capacity of 1.5 kg is useful for carrying small parts, tools, or components. The selected ring magnet (N35) has a thickness of 15 mm. However, due to market availability, a ring magnet with an Outer Diameter (OD) of 50 mm, an ID of 10 mm, and a thickness of 12.5 mm is selected for the design. The selected SOD is 0.5 mm, and based on these values, the magnetic wheel is designed so that the magnet will always have a stand-off distance of 0.5 mm when it is in contact with the surface, as shown in Figure 5.

The magnetic wheel that has been designed is composed of two modules which form the wheel and establish the SOD. Aluminium 6061 is used to hold the ring magnet due to its lightweight strength and ability to facilitate the handling of the permanent magnet. Aluminium 6061 offers an advantage over ferromagnetic materials as it eases the placement and detachment of the magnets from the wheel. Figure 6 shows the solid model of the magnetic wheel for cilampi in an exploded view. The cilampi robot is designed with flexibility in mind, able to carry either a camera for visual inspections or an ultrasonic probe for checking structural integrity. While it can only carry one sensor at a time, its modular setup allows for easy swapping depending on the task at hand. This makes the robot adaptable, whether you're using it for visual inspections of pipeline surfaces or ultrasonic testing to detect cracks and corrosion.
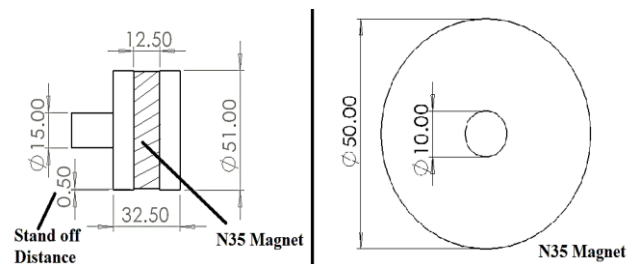

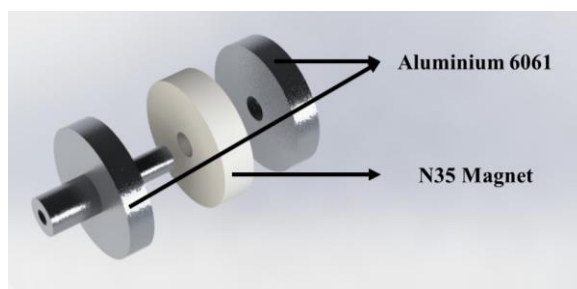Figure 5. Magnetic wheel dimensions

Figure 6. Exploded view of the magnetic wheel for cilampi

A FEMM simulation was conducted to determine the magnetic adhesion force produced by the ring magnet against a ferromagnetic surface. Two ring magnets were placed 0.5 mm from the ferromagnetic surface, having a thickness of 2 mm and an outer diameter of 400 mm. Figure 7 shows the model and material assignment for two magnetic wheels placed on the ferromagnetic surface. The simulation results show that using multiple magnets can be more effective in generating a stronger magnetic adhesion force compared to using a single magnet. The magnetic adhesion force generated by two magnets is 88.39 N (9 Kg). Figure 8 shows the results of the simulation studies.
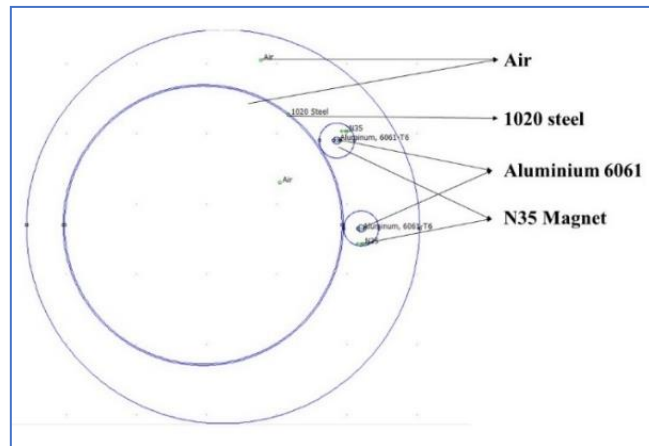
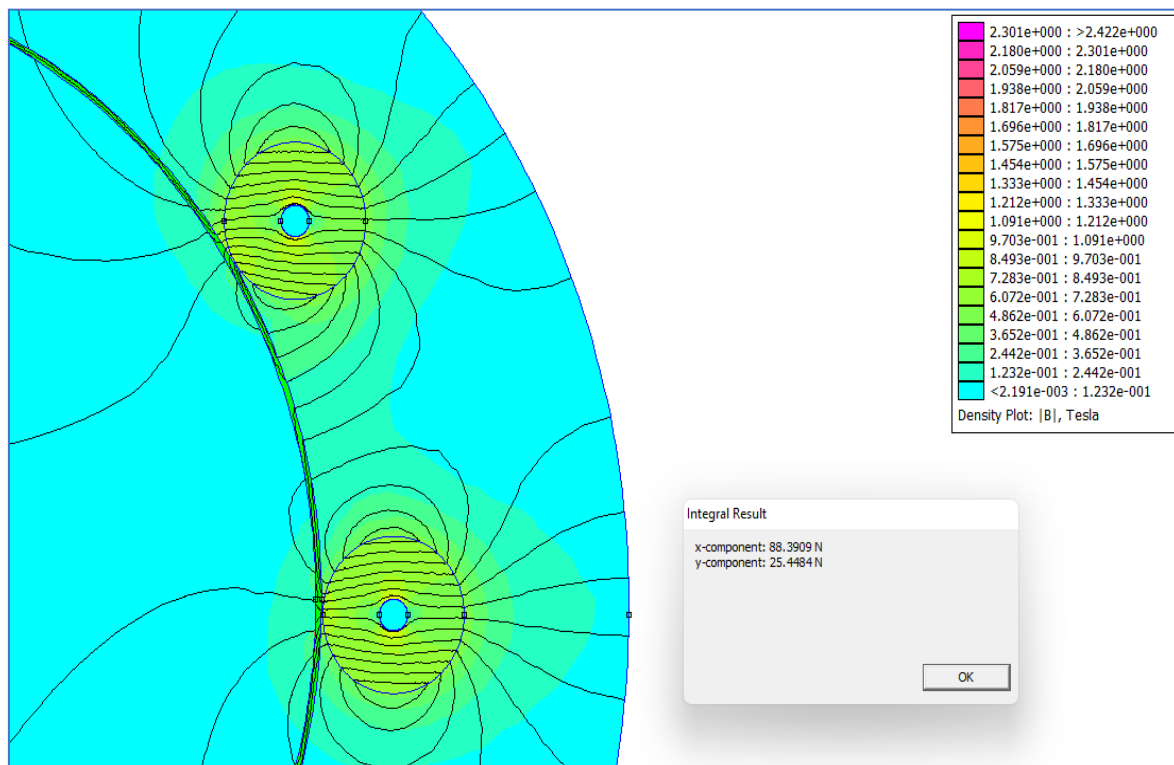Figure 7. FEMM Model of two magnetic wheels against the ferromagnetic surface

Figure 8. Flux distribution of two magnets

4. DESIGN OF CILAMPI

Previous studies [6]–[8] show that pipeline inspection robots are usually designed to match the pipe's circumference, which makes them larger. As the pipe diameter increases, the robot size also increases. To solve this problem, a compact robot is needed that can adjust to different pipeline diameters without changing its size. The prototype of this robot was designed and modeled in SolidWorks. The goal was to create a small, lightweight out-pipe inspection robot with magnetic wheels. This robot can climb vertical pipes while carrying its own weight and extra load if needed. The main parts of the robot are the chassis, motor mounting bracket, motor, and magnetic wheels, as shown in Figure 9. The robot's design is centered around its chassis, which is the main body. The chassis holds the motor mounting bracket, motor, and magnetic wheels securely in place. Cilampi is a differential drive robot with two wheels that are not in a straight line (non-co-linear). The wheels are placed with a small shift in both lateral and longitudinal directions. This helps the robot move better and adjust to the curved pipeline surface. The following are the assumptions and parameters used in design and simulation: The pipe is cylindrical with a minimum outer

diameter of 200 mm, the coefficient of friction between Aluminium and Mild steel is 0.61, Magnet is placed at a constant Standoff distance of 0.5 mm.
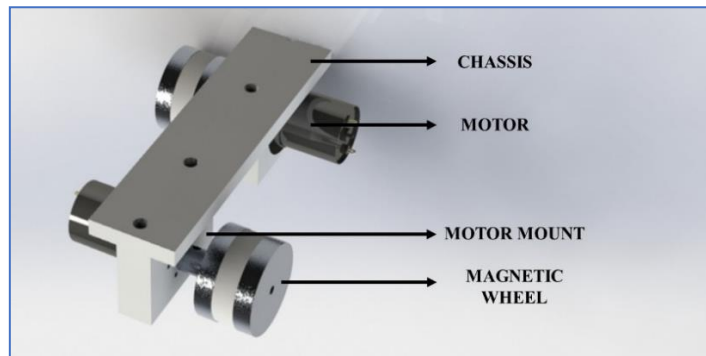

Figure 9. Design and key components of the cilampi out-pipe inspection robot

Cilampi features two wheels—one on each side—for balanced support, reduced weight, and space for sensors. Using a 400 mm diameter pipe as reference, optimal wheel spacing was determined by adjusting the 70 mm motor mounts to avoid contact with the pipe surface, resulting in a 56 mm gap between them. This setup yields an ideal wheel center-to-center distance of 130 mm, ensuring continuous surface contact and stability. Each wheel provides a magnetic adhesion force of 4.7 kg. The robot's total weight, calculated in SolidWorks, is 0.98 kg. With the chassis finalized, motor torque requirements are next to be calculated.

5.   KINEMATICS OF THE DIFFERENTIAL DRIVE MOBILE ROBOT WITH NON-CO-LINEAR WHEELS

Cilampi is a differential drive mobile robot with wheels that are Non-Co-Linear (NCL), having an offset in both y- and x–axis as illustrated in Figure 10. Thus, the kinematic model of cilampi differs from the traditional models. Which is given as follows.
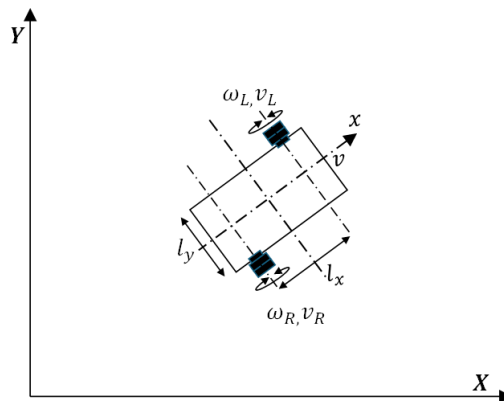

Figure 10. The differential drive mobile robot with wheels that are not co-linear, exhibiting an offset in both the y-axis (wheelbase distance) and the x-axis (lateral offset)

Let v – Linear velocity of the robot; ω – Angular velocity of the robot; x, y – position of the robot w.r.t the global frame; θ - Orientation of the robot; X, Y - the fixed global frame. R – Wheel radius; l_y – the distance between the wheels along the Y-axis; l_x – the distance between the wheels along the X-axis; C – Chord length of the pipe; v_L, v_R – the linear velocity of the left and right wheels, respectively; ω_L, ω_R – the angular velocity of the left and right wheels, respectively.

We know that the linear velocity 'v' is given by (1),

$$v = \frac{v_L + v_R}{2} \tag{1}$$

where, $v_L = R.\omega_L$ and $v_R = R.\omega_R$. The effective radius L_{eff} to the instantaneous center of rotation (ICR), accounting for both wheel offsets, is given by (2).

$$L_{eff} = \sqrt{\left(\frac{l_x}{2}\right)^2 + \left(\frac{l_y}{2}\right)^2} \tag{2}$$

Angular velocity of the robot is determined by the relative velocities of the wheels and is given by (3).

$$\omega = \left(\frac{v_R - v_L}{L_{eff}}\right) \tag{3}$$

From (1), (2), and (3), the global motion equations could be framed as (1).

$$\begin{aligned}
\dot{x} &= v\cos\theta - \omega\, l_x \sin\theta \\
\dot{y} &= v\sin\theta + \omega\, l_x \cos\theta \\
\dot{\theta} &= \omega
\end{aligned} \tag{4}$$

Equation (4) gives the robot's position and orientation in the global frame. The term $\omega\, l_x$ It is used for adjusting the offset of the wheel along the x-axis. This shows how the NCL arrangement affects the motion of the robot. The above kinematic model demonstrates how the NCL wheel configuration modifies the motion behavior compared to conventional differential drive robot motion introducing offsets along both axes, the robot maintains continuous contact with curved surfaces, improving grip, stability, and adherence, particularly when navigating along cylindrical pipes. The inclusion of the l_x, the motion equations ensures that trajectory estimation remains accurate during rotation and curved traversal.

6. DYNAMIC SIMULATION OF CILAMPI

The payload capacity of the robot is determined through dynamic analysis. The analysis requires certain specifications as inputs, such as the material properties of the magnetic wheel (Aluminium 6061) and the robot body (PLA). Additionally, the motor speed is set to 20 RPM, and the magnetic adhesion force is given as 46.11 N for each magnetic wheel. The simulation environment involves the robot and a vertical wall, with the robot carrying a payload as it moves along the wall.

Figure 11 shows the payload-carrying capacity of cilampi. First, the robot was tested with only its weight (self-weight 0.98 kg), and it was observed that the necessary torque to carry a payload of 0.98 kg was 0.07 Nm. In the subsequent simulation, the robot's payload was increased (including self-weight) by 1.5 kg, and it was observed that the necessary torque increased to 0.12 Nm. Beyond the payload of 1.5 kg, the robot begins to lose traction and slip. The simulation results indicate that the robot can carry its self-weight of 0.98 kg plus an additional payload of up to 0.52 kg for a total weight of 1.5 kg, with a necessary torque of 0.12 Nm. Beyond this weight limit, the robot begins to experience slipping, indicating that it is unable to carry the load effectively.
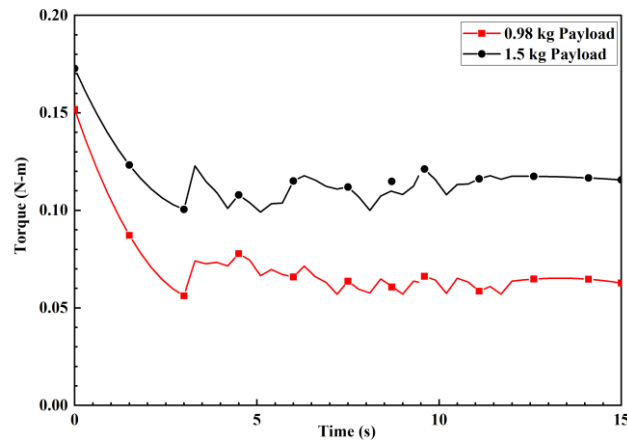
Figure 11. Payload carrying capacity of cilampi

7.   EXPERIMENTAL TEST OF MAGNETIC ADHESION OF RING MAGNETS

Cilampi is developed through 3D printing technology with Polylactic Acid (PLA) as material, as shown in Figure 12. It consists of two magnetic wheels. The wheel modules have a larger diameter than the ring magnet (N35), which ensures that the SOD is always 0.5 mm between the magnet and ferromagnetic surface, preventing the magnet from adhering directly to the surface. The robot is designed with modular parts, making it easy to replace them if necessary. The Rhino GB37 12 V motor, used in the robot, draws 300 mA of current per motor. Since the robot uses two motors, the total current consumption from the motors is 600 mA, which translates to a power consumption of 7.2 W (12 V × 0.6 A). The L298N motor driver adds 0.72 W. The ESP32-CAM module, used for inspection, consumes 0.9 W when the flash is off. In total, the robot's power consumption comes to 8.82 W. The robot is powered by a 2200 mAh 1S LiPo battery, which provides about 8.14 Wh (3.7 V × 2.2 Ah) of energy. Under ideal conditions, this battery would last around 55 minutes of continuous operation. However, taking into account real-world inefficiencies, such as power losses in the motor driver and battery, the expected battery life is closer to 44 minutes.

Figure 12. Cilampi prototype

To validate the simulation results, a pull-up load test as illustrated in Figure 13 is conducted using an N35 ring magnet (OD 50 mm, ID 10 mm, thickness 12.5 mm). The setup includes a loading screw connected to a weighing scale, with the magnet attached to the scale's hook. In the first test, the magnet is placed 0.5 mm above a 2 mm-thick surface, and the maximum pull force is recorded. In the second test, the prototype is placed on a ferromagnetic pipe to measure adhesion force. Experimental results are summarized in Table 1.
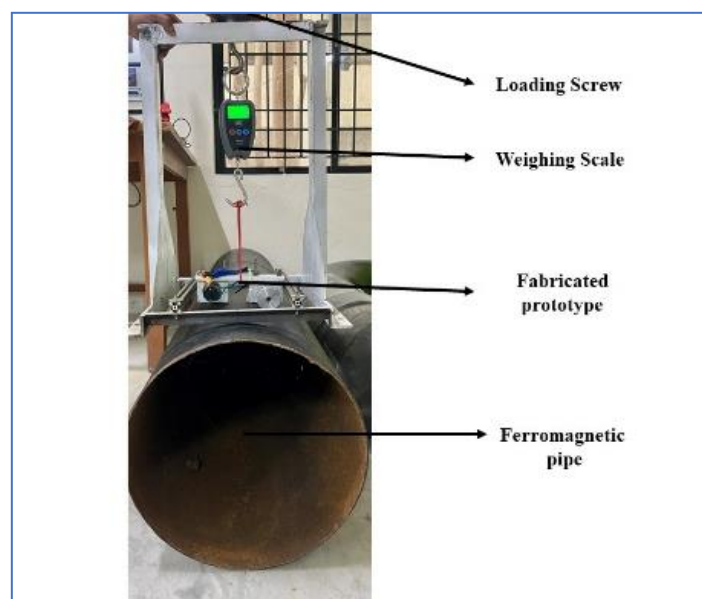

Figure 13. Experimental setup to measure the adhesion force of two magnets

Table 1. Experimental results of magnetic adhesion of ring magnets

Test Sets	No. of ring magnets	Adhesion force (N)	Experimental adhesion force (N)	Error (%)
1	1	46.11	42.57	8.31
2	2	88.39	81.69	8.2
		Total Average Error (AT)		8.25

The adhesion force of a single magnet is measured to be 42.57 N (4.34 Kg). The experimental and simulated results have an error rate of 8.31 %. In the second experiment, the adhesion force of two magnets is measured, and the entire robot needs to be used due to the requirement of positioning the two magnets 0.5 mm apart in the pipeline's circumferential direction. The result shows that the adhesion force of the magnet along with the robot is 70.9 N (7.23 kg). Taking into account the self-weight of the robot, which is 10.79 N (1.1 kg), the total adhesion force of the two magnets is found to be 81.69 N (8.33 Kg). The experimental and simulated results have an error rate of 8.2 %. Thus, the total average error between results is about 8.25 %.

The load testing of Cilampi, shown in Figure 14, demonstrates it can carry a 0.35 kg payload (excluding its 1.1 kg self-weight), with a simulation-experiment error of 3.33%. Magnetic wheels enable movement on vertical ferromagnetic pipes, and an onboard camera helps detect corrosion. Stability tests in various static orientations confirm it supports its own weight without slipping. As shown in Figure 15, Cilampi moves along a 400 mm diameter, 2 mm thick pipe, both in circular and vertical screw-type paths. A demonstration video is available at https://youtu.be/w2PNFEVP61Y.
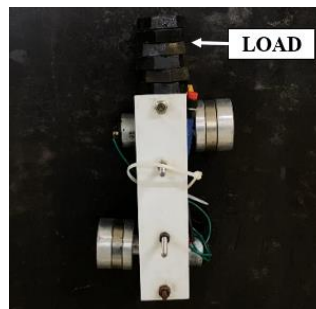

Figure 14. Load test on cilampi

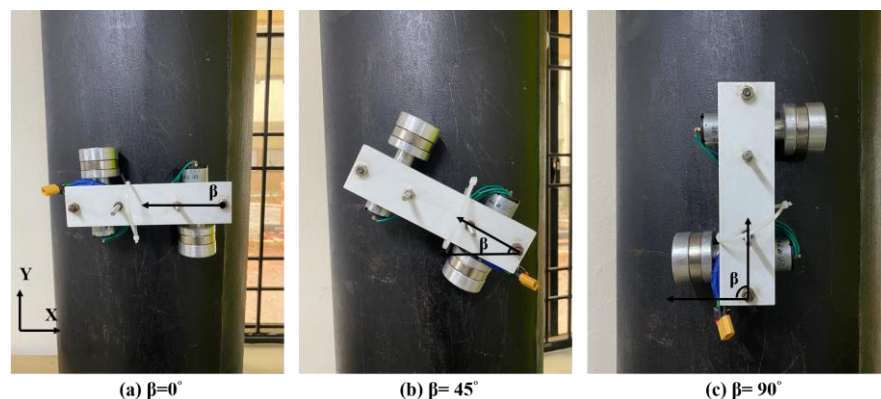(a) β=0°   (b) β= 45°   (c) β= 90°

Figure 15. Cilampi placed at different orientations on a vertical pipe

8.   DISCUSSION

Out-pipe inspection robots employ various adhesion mechanisms, including pneumatic, magnetic, mechanical, vacuum suction, combined, and bio-inspired methods. Pneumatic adhesion [28] uses controlled air pressure in soft actuators for smooth surface mobility. Magnetic adhesion [29], especially with permanent magnets, provides strong, power-free grip on ferromagnetic surfaces. Mechanical adhesion uses clamps or grips for broad surface compatibility. Combined methods improve adaptability and payload but increase

system complexity [30]. Vacuum suction is effective on smooth, sealed surfaces but less reliable on uneven ones. Bio-inspired adhesion, modeled after natural climbers like geckos, offers flexibility but faces limitations in payload and design complexity.

Table 2 presents a comparison of these methods. From this comparison, permanent magnetic adhesion emerges as the most balanced option for pipeline inspection, combining high payload capacity, design simplicity, and reliable performance on ferromagnetic pipes. Ultimately, the right adhesion method depends on the specific pipeline conditions and inspection needs. In the case of pipelines, especially those made from ferromagnetic materials, magnetic adhesion is a natural choice for an effective and efficient inspection robot design.

Table 2. Adhesion methods comparison

Adhesion methods	Design complexity	Surface type	Payload
Pneumatic adhesion	High	Smooth surface	Medium
Magnetic adhesion	Medium	Ferromagnetic surface	High
Mechanical adhesion	Medium	Any surface	Medium
Combined adhesion	High	Any surface	High
Vacuum suction	Medium	Smooth, non-porous	Medium
Bio-inspired adhesion	High	Various surfaces	Low to medium

The proposed Cilampi robot uses ring-type permanent magnets for magnetic adhesion in external pipeline inspection. Design optimization through FEMM simulations showed that increasing magnet thickness and reducing ID enhance adhesion, with the best configuration (OD: 50 mm, ID: 10 mm, thickness: 15 mm) yielding 62.72 N. A stand-off distance of 0.5 mm further maximized adhesion, while wall thickness beyond 8 mm had minimal effect. Using two magnets increased adhesion to 81.69 N experimentally. Dynamic simulations confirmed the robot could carry up to 1.5 kg (including self-weight) with a torque requirement of 0.12 Nm; slippage occurred beyond this. Cilampi achieved stable vertical climbing with a screw-like motion, and experimental results closely matched simulations, with errors of 8.25% (adhesion) and 3.33% (load).

Despite its strengths, Cilampi currently supports only ferromagnetic pipelines ≥ 200 mm in diameter. The use of rubber on wheels to enhance friction presents challenges due to deformation affecting SOD and reducing effective adhesion. Cilampi is compared with the existing systems and is benchmarked based on its performance, as shown in Table 3.

Table 3. Comparison with existing systems

Parameters	Omniclimber I [31]	Magnebike [23]	Cilampi
Self-weight (w/o controller and battery)	1.099 Kg	3.5 Kg	0.98 Kg
Pipeline diameter adaptability	≥ 300 mm	≥ 200 mm	≥ 200 mm
Adhesion force	20.13 N	250 N	81.69 N
No. magnets used	16	2	2
Magnetic wheel type	Omni-Directional Wheels	Straight wheels	Straight wheels

The comparison shows that Cilampi stands out as the lightest out-pipe inspection robot at just 0.98 kg, while achieving a strong magnetic adhesion force of 81.69 N using only two ring magnets. Its simple and efficient magnetic wheel design allows reliable operation on ferromagnetic pipelines with diameters of 200 mm and above. Compared to existing OPIRs, Cilampi offers an optimal balance of lightweight construction, effective adhesion, and adaptability, making it a robust and practical solution for external pipeline inspection.

9. CONCLUSION

This paper presents Cilampi, a modular magnetic wheeled outer pipe inspection robot (OPIR) designed for ferromagnetic pipelines. A key contribution is the optimized magnetic wheel design—specifically, increasing magnet thickness, reducing ID, and maintaining a stand-off distance (SOD) of 0.5 mm—which significantly improved adhesion. Experimental results showed that two magnets achieved an adhesion force of 81.69 N, enabling the robot to carry up to 1.5 kg (including self-weight) and operate for approximately 44 minutes per charge. Cilampi demonstrated reliable climbing and navigation over vertical pipes using a screw-like motion, with adhesion and load capacity errors of 8.25% and 3.33%, respectively. However, limitations include compatibility only with ferromagnetic surfaces and pipes ≥200 mm in diameter.

Future work will focus on miniaturization for smaller pipes and improving traction by addressing the challenges posed by rubber elasticity affecting SOD. Enhancing energy efficiency is another priority. Strategies include implementing power-saving modes for the ESP32-CAM, using PWM for motor control, and potentially integrating energy-harvesting methods. Selective sensor activation and a robust battery management system could further extend operation time. Additionally, incorporating AI-based defect detection—using visual and ultrasonic data—could enable autonomous pipeline condition assessment, improve inspection accuracy, and reduce manual oversight.

REFERENCES

[1] T. Yamamoto, S. Sakama, and A. Kamimura, "Pneumatic duplex-chambered inchworm mechanism for narrow pipes driven by only two air supply lines," *IEEE Robotics and Automation Letters*, vol. 5, no. 4, pp. 5034–5042, Oct. 2020, doi: 10.1109/LRA.2020.3003859.

[2] R. S. Elankavi, D. Dinakaran, R. M. Kuppan Chetty, M. M. Ramya, and A. S. Arockia Doss, "Kinematic modeling and analysis of wheeled in-pipe inspection mobile robot," in *Handbook of Smart Materials, Technologies, and Devices: Applications of Industry 4.0*, Springer, 2022, pp. 995–1009.

[3] C. Choi, B. Park, and S. Jung, "The design and analysis of a feeder pipe inspection robot with an automatic pipe tracking system," *IEEE/ASME Transactions on Mechatronics*, vol. 15, no. 5, pp. 736–745, Oct. 2010, doi: 10.1109/TMECH.2009.2032541.

[4] S. H. Lee, "Design of the out-pipe type pipe climbing robot," *International journal of precision engineering and manufacturing*, vol. 14, no. 9, pp. 1559–1563, 2013.

[5] Se-gon Roh and Hyouk Ryeol Choi, "Differential-drive in-pipe robot for moving inside urban gas pipelines," *IEEE Transactions on Robotics*, vol. 21, no. 1, pp. 1–17, Feb. 2005, doi: 10.1109/TRO.2004.838000.

[6] Y.-S. Kwon and B.-J. Yi, "Design and motion planning of a two-module collaborative indoor pipeline inspection robot," *IEEE Transactions on Robotics*, vol. 28, no. 3, pp. 681–696, Jun. 2012, doi: 10.1109/TRO.2012.2183049.

[7] R. S. Elankavi, "Developments in inpipe inspectionrobot: a review," *Journal of Mechanics of Continua and Mathematical Sciences*, vol. 15, no. 5, May 2020, doi: 10.26782/jmcms.2020.05.00022.

[8] R. S. Elankavi, D. Dinakaran, R. M. K. Chetty, M. M. Ramya, and D. G. H. Samuel, "A review on wheeled type in-pipe inspection robot," *International Journal of Mechanical Engineering and Robotics Research*, vol. 11, no. 10, pp. 745–754, 2022, doi: 10.18178/ijmerr.11.10.745-754.

[9] M. H. Ali, T. Zharakhmet, M. Atykhan, A. Yerbolat, and S. Batai, "Development of a robot for boiler tube inspection," in *Proceedings of the 15th International Conference on Informatics in Control, Automation and Robotics*, SCITEPRESS - Science and Technology Publications, 2018, pp. 534–541. doi: 10.5220/0006930205340541.

[10] B. Chu, K. Jung, C.-S. Han, and D. Hong, "A survey of climbing robots: locomotion and adhesion," *International Journal of Precision Engineering and Manufacturing*, vol. 11, no. 4, pp. 633–647, Aug. 2010, doi: 10.1007/s12541-010-0075-3.

[11] S. Nansai and R. Mohan, "A survey of wall climbing robots: recent advances and challenges," *Robotics*, vol. 5, no. 3, p. 14, Jul. 2016, doi: 10.3390/robotics5030014.

[12] X. Hou *et al.*, "Space climbing robot feet with microarray structure based on discrete element method," *International Journal of Robotics and Automation*, vol. 34, no. 1, 2019, doi: 10.2316/J.2019.206-5096.

[13] P. Chattopadhyay and S. K. Ghoshal, "Adhesion technologies of bio-inspired climbing robots: a survey," *International Journal of Robotics and Automation*, vol. 33, no. 6, 2018, doi: 10.2316/Journal.206.2018.6.206-5193.

[14] A. Brusell, G. Andrikopoulos, and G. Nikolakopoulos, "A survey on pneumatic wall-climbing robots for inspection," in *2016 24th Mediterranean Conference on Control and Automation (MED)*, IEEE, Jun. 2016, pp. 220–225. doi: 10.1109/MED.2016.7535885.

[15] F.-W. Bach, M. Rachkov, J. Seevers, and M. Hahn, "High tractive power wall-climbing robot," *Automation in Construction*, vol. 4, no. 3, pp. 213–224, Oct. 1995, doi: 10.1016/0926-5805(95)00005-L.

[16] C. Balaguer, A. Gimenez, and C. Abderrahim, "ROMA robots for inspection of steel based infrastructures," *Industrial Robot: An International Journal*, vol. 29, no. 3, pp. 246–251, Jun. 2002, doi: 10.1108/01439910210425540.

[17] J. Jose, R. S. Elankavi, D. Dinakaran, R. M. K. Chetty, and M. M. Ramya, "Investigations on the magnetic adhesion properties of pipe surface inspection robot," 2022, p. 030004. doi: 10.1063/5.0108495.

[18] Z. Yu, Y. Shi, J. Xie, S. X. Yang, and Z. Dai, "Design and analysis of a bionic adhesive foot for gecko robot climbing the ceiling," *International Journal of Robotics and Automation*, vol. 33, no. 4, 2018, doi: 10.2316/Journal.206.2018.4.206-5412.

[19] M. A. Fanni, M. G. Alkalla, and A. Mohamed, "Propeller-type skid steering climbing robot based on a hybrid actuation system," *International Journal of Robotics and Automation*, vol. 33, no. 3, 2018, doi: 10.2316/Journal.206.2018.3.206-5017.

[20] S. Lai, D. Y. Chen, H. Chen, and Y. W. Fu, "Pulsed eddy current testing of inner wall flaws in pipe under insulation," *Procedia Engineering*, vol. 130, pp. 1658–1664, 2015, doi: 10.1016/j.proeng.2015.12.334.

[21] J. Jose, R. Sugin Elankavi, D. Dinakaran, R. M. Kuppan Chetty, and M. M. Ramya, "A comparative study of adhesion mechanism for wall climbing robots: ring magnet vs. block magnets," *IOP Conference Series: Materials Science and Engineering*, vol. 1145, no. 1, p. 012063, Apr. 2021, doi: 10.1088/1757-899X/1145/1/012063.

[22] M. Tavakoli, L. Marques, and A. T. de Almeida, "Development of an industrial pipeline inspection robot," *Industrial Robot: An International Journal*, vol. 37, no. 3, pp. 309–322, May 2010, doi: 10.1108/01439911011037721.

[23] F. Tâche, W. Fischer, G. Caprari, R. Siegwart, R. Moser, and F. Mondada, "Magnebike: a magnetic wheeled robot with high mobility for inspecting complex-shaped structures," *Journal of Field Robotics*, vol. 26, no. 5, pp. 453–476, May 2009, doi: 10.1002/rob.20296.

[24] "Finite element method magnetics: homepage." Accessed: Jan. 10, 2022. [Online]. Available: https://www.femm.info/wiki/HomePage

[25] W. Fischer, F. Tâche, and R. Y. Siegwart, "Magnetic wall climbing robot for thin surfaces with specific obstacles," in *6th International Conference on Field and Service Robotics-FSR 2007*, 2007, pp. 1–11.

[26] eSUN, "3D printing materials worldwide leading brand." Accessed: Jan. 10, 2022. [Online]. Available: https://www.esun3d.com/

[27] R. Wang and Y. Kawamura, "An automated sensing system for steel bridge inspection using GMR sensor array and magnetic wheels of climbing robot," *Journal of Sensors*, vol. 2016, pp. 1–15, 2016, doi: 10.1155/2016/8121678.

[28] L. Dai, J. Wang, Z. Liu, and Y. Fei, "Out-pipe climbing soft robot with omnidirectional actuator," in *2020 3rd World Conference on Mechanical Engineering and Intelligent Manufacturing (WCMEIM)*, IEEE, Dec. 2020, pp. 56–60. doi:

10.1109/WCMEIM52463.2020.00018.

[29] W. A. Blyth, D. R. W. Barr, and F. Rodriguez y Baena, "A reduced actuation mecanum wheel platform for pipe inspection," in *2016 IEEE International Conference on Advanced Intelligent Mechatronics (AIM)*, IEEE, Jul. 2016, pp. 419–424. doi: 10.1109/AIM.2016.7576803.

[30] Y. Jiang, D. Chen, H. Zhang, F. Giraud, and J. Paik, "Multimodal pipe-climbing robot with origami clutches and soft modular legs," *Bioinspiration & Biomimetics*, vol. 15, no. 2, p. 026002, Jan. 2020, doi: 10.1088/1748-3190/ab5928.

[31] M. Tavakoli, C. Viegas, L. Marques, J. N. Pires, and A. T. de Almeida, "OmniClimbers: omni-directional magnetic wheeled climbing robots for inspection of ferromagnetic structures," *Robotics and Autonomous Systems*, vol. 61, no. 9, pp. 997–1007, Sep. 2013, doi: 10.1016/j.robot.2013.05.005.

FUNDING INFORMATION

AUTHOR CONTRIBUTIONS STATEMENT

This journal uses the Contributor Roles Taxonomy (CRediT) to recognize individual author contributions, reduce authorship disputes, and facilitate collaboration.

Name of Author	C	M	So	Va	Fo	I	R	D	O	E	Vi	Su	P	Fu
Sugin Elankavi Rajendran	✓	✓	✓	✓	✓	✓		✓	✓	✓			✓	
Kuppan Chetty Ramanathan		✓		✓	✓		✓			✓	✓	✓	✓	✓
Harish Kumar Guasekaran		✓			✓			✓	✓	✓				
Arun Kumar Pinagapani		✓			✓			✓	✓	✓				
Dinakaran Devaraj		✓		✓	✓		✓			✓	✓	✓	✓	✓
Ramya Mathanagopal		✓		✓			✓			✓	✓	✓	✓	

CONFLICT OF INTEREST STATEMENT

The authors state there is no conflict of interest.

DATA AVAILABILITY

Data availability does not apply to this paper as no new data were created or analyzed in this study.

BIOGRAPHIES OF AUTHORS

Sugin Elankavi Rajendran is an assistant professor and head of the centre for industrial automation at the Chennai Institute of Technology. He earned his Ph.D. in robotics and automation from Hindustan University, Chennai, in 2023. His research interests include mobile robots, mechatronics, and condition monitoring, with a primary focus on pipeline inspection robots. He holds an M.E. in manufacturing engineering (2019) and a B.E. in mechanical engineering (2017) from Anna University. Dr. Rajendran is an active member of the IEEE robotics and automation society (RAS), India, and collaborates on industry-sponsored research projects in robotics and automation. He can be contacted at suginelankavir@citchennai.net.

Kuppan Chetty Ramanathan received his Ph.D. degree in robotics and controls from the Indian Institute of Technology Madras (IIT Madras) in 2010, his M.Tech. degree in sensor systems technology from Vellore Institute of Technology, Vellore, in 2004, and his B.Tech. degree in instrumentation and control engineering from Madurai Kamaraj University, Tamil Nadu, India, in 2002. Currently, he serves as a professor in the school of mechanical engineering at SASTRA Deemed University. His career spans more than 20 years across both academia and industry, with a focus on robotics, mechatronics, and automation. His research interests include cooperative and intelligent robotics, climbing, assistive and rehabilitation robotics, industrial automation, and mechatronic systems. He can be contacted at rmkuppan@gmail.com.

Harish Kumar Guasekaran is currently pursuing a B.Tech. degree in mechatronics at SASTRA Deemed to be University, Thanjavur, Tamil Nadu, India. He can be contacted at 126012020@sastra.ac.in.

Arun Kumar Pinagapani received his Ph.D. from Anna University, M.E. in control systems from PSG college of technology, and B.Tech. in EIE from SASTRA University. He is an assistant professor - III at SASTRA University, specializing in control and automation, soft computing, and industrial automation. His research focuses on intelligent control systems and automation. He can be contacted at arunkumar@eie.sastra.edu.

Dinakaran Devaraj is the director of R&D and engineering at Haystack Robotics, Chennai. He received his B.E. in mechanical engineering in 2001, M.E. in manufacturing engineering in 2004, and Ph.D. in industrial automation from Anna University, Chennai. With over 20 years of experience, he has led R&D projects across defense, manufacturing, transportation, and medical sectors. His expertise includes robotics, CNC controls, and condition monitoring. He is also an executive member of the condition monitoring society of India. He can be contacted at drddinakaran@gmail.com.

Ramya Mathanagopal is a seasoned academic and researcher with over 20 years of expertise in artificial intelligence, soft computing, and image processing. She currently serves as the dean of Agurchand Manmull Jain College, Chennai. A Ph.D. graduate from Madurai Kamaraj University (2010), she formerly served at the Centre for Automation and Robotics (ANRO), Hindustan Institute of Technology & Science. Dr. Ramya has authored 35+ research publications and led several DRDO-funded projects, including underwater image enhancement and tactical warfare training systems. Beyond her research, she is an active contributor to the academic community, frequently invited to deliver lectures, conduct training workshops, and chair sessions at national and international conferences. He can be contacted at prof.mm.ramya@gmail.com.